CHEMISTRY OF MATERIALS

pubs.acs.org/cm Article

Selectivity between SiO_2 and SiN_x during Thermal Atomic Layer Etching Using $Al(CH_3)_3$/HF and Spontaneous Etching Using HF and Effect of HF + NH_3 Codosing

Published as part of Chemistry of Materials virtual special issue "Precision Patterning".

Marcel Junige* and Steven M. George

Cite This: *Chem. Mater.* 2024, 36, 6950–6960 Read Online

ACCESS | Metrics & More | Article Recommendations | Supporting Information

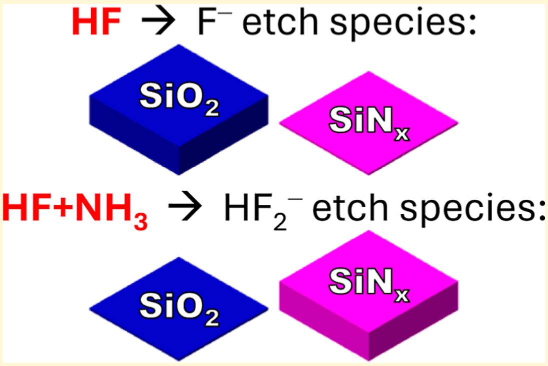

ABSTRACT: Selectivity was examined between SiO_2 and SiN_x during thermal atomic layer etching (ALE) and spontaneous etching. Thermal ALE of SiO_2 and SiN_x was explored using sequential trimethylaluminum (TMA) and hydrogen fluoride (HF) with reactant exposures of 3 Torr for 45 s at 275 °C. SiO_2 thermal ALE achieved an etch per cycle (EPC) of 0.20 Å/cycle and near-ideal synergy up to 95%. SiN_x thermal ALE exhibited a higher EPC of 1.06 Å/cycle. The selectivity factor was ~5:1 for SiN_x etching compared to SiO_2 etching (preferential SiN_x removal) during thermal ALE using TMA and HF. Spontaneous etching was then quantified using repeated exposures of HF vapor alone at 3 Torr and 275 °C. SiO_2 spontaneous etching was minor at an etch rate of 0.03 Å/min, enabling near-ideal synergy for SiO_2 thermal ALE. In contrast, major SiN_x spontaneous etching displayed an etch rate of 1.72 Å/min and predominated over SiN_x thermal ALE. The selectivity factor was ~50:1 for SiN_x spontaneous etching compared to SiO_2 spontaneous etching using an HF pressure of 3 Torr. This selective SiN_x spontaneous etching was attributed to F^- surface species during HF exposures. NH_3 codosing with HF was then examined during thermal ALE and spontaneous etching. Thermal ALE of SiO_2 and SiN_x was examined using sequential TMA and HF + NH_3 codosing with reactant exposures of 3 Torr for 45 s at 275 °C. SiO_2 thermal ALE with HF + NH_3 codosing had a high EPC of 8.83 Å/cycle. In contrast, SiN_x thermal ALE with HF + NH_3 codosing was negligible. The selectivity factor was reversed and much higher at >1000:1 for SiO_2 etching compared to SiN_x etching (preferential SiO_2 removal) during thermal ALE with HF + NH_3 codosing. Rapid SiO_2 spontaneous etching with HF + NH_3 codosing at 3 Torr had an etch rate of 27.50 Å/min. In contrast, SiN_x spontaneous etching with HF + NH_3 codosing produced a very low etch rate of 0.02 Å/min. The selectivity factor was >1000:1 for SiO_2 spontaneous etching compared to SiN_x spontaneous etching with HF + NH_3 codosing. This selective SiO_2 spontaneous etching was attributed to HF_2^- surface species during HF + NH_3 exposures. These studies revealed that the NH_3 coadsorbate during HF exposures modified the active etch species and dramatically influenced the etch selectivity between SiO_2 and SiN_x. Reciprocal etch selectivity should be important for the selective removal of SiO_2 or SiN_x in composite structures.

1. INTRODUCTION

Microelectronics processing methods are being challenged by sub-10 nm technology node requirements to fabricate advanced, three-dimensional (3D) device structures.[1] Overcoming the limits of top-down patterning requires breakthroughs in nanomanufacturing techniques. Novel bottom-up, self-aligned approaches provide a crucial solution by eliminating lithographic photomasks and associated edge-placement errors.[2] Self-alignment methods include area-selective deposition or etching for a range of materials.[3−5]

Etch selectivity may remove one specific material while leaving intact other materials in proximity.[5] The development of selectivity between similar materials, such as silicon (Si)-based dielectrics, is a particular challenge. This challenge motivated the current study of selective etching of silicon dioxide (SiO_2) with the retention of silicon nitride (SiN_x), and the reciprocal challenge of selective SiN_x etching while retaining SiO_2. This etch selectivity should be useful for the selective removal of sacrificial SiO_2 or SiN_x in composite structures that are employed for fabricating devices such as 3D NAND.[6,7]

Etching can be accomplished by wet or dry methods. Wet etching in solution can suffer from pattern collapse due to the

Received: April 8, 2024
Revised: May 31, 2024
Accepted: June 7, 2024
Published: July 1, 2024

ACS Publications

https://doi.org/10.1021/acs.chemmater.4c01040

forces of capillary action.[8] In contrast, dry, gas-phase methods can achieve distortion-free profiles for miniaturized, high-density patterns. Anisotropic, vertical pattern transfer relies on directional reactive ion etching using plasmas.[9−12] However, ion etching typically roughens and damages the surface to depths of several nanometers.[13,14] In contrast, thermally activated dry etching processes yield minimal damage to underlying materials.

Atomic layer control of dry thermal etching can be obtained using atomic layer etching (ALE) methods.[15−18] ALE employs an alternating sequence of separate self-limiting surface reactions. The first reaction typically modifies the surface and the second reaction volatilizes the modified surface layer.[19] Thermal ALE processes have been developed for a variety of Si-containing materials such as Si,[20] SiO_2,[20−22] Si_3N_4,[23] and silicon−germanium (SiGe).[24]

Figure 1 illustrates the surface chemistry for SiO_2 thermal ALE. This chemistry combines ligand-exchange and conversion reactions by trimethylaluminum [TMA, $Al(CH_3)_3$] together with fluorination by hydrogen fluoride (HF). The TMA reaction removes an AlF_3 surface layer by ligand exchange,[25,26] producing volatile $Al_2F_x(CH_3)_y$ dimers and $Al_3F_x(CH_3)_y$ trimers.[27,28] At sufficient TMA exposures, TMA also converts the SiO_2 surface into a mixture of Al_2O_3, aluminosilicate, and reduced Si species. Methyl groups terminate the converted $AlSi_xO_y$ surface layer.[21,22] The conversion reaction produces tetramethylsilane [$Si(CH_3)_4$] as a volatile product. SiO_2 surfaces need this conversion because SiO_2 by itself has no direct etch pathway by fluorination and ligand-exchange reactions at lower TMA exposures in the absence of conversion.[29] HF then fluorinates the Al_2O_3 surface, forming an AlF_3 surface layer.[30] The fluorination reaction produces methane (CH_4) and water (H_2O) as volatile products.[27]

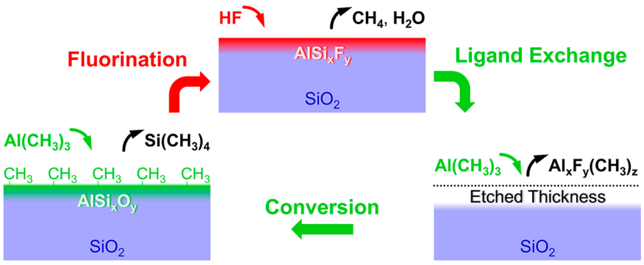

Figure 1. Schematic for SiO_2 thermal ALE based on sequential TMA and HF exposures that perform the reactions: ligand-exchange by TMA; conversion by TMA; and fluorination by HF.

The benefits of thermal ALE depend on the self-limiting characteristics of each reaction step. A problem can occur when spontaneous etch pathways continuously remove the targeted material. A synergy factor has been introduced to quantify the ideality of an ALE sequence that alternates between separate A and B reactions compared with repeating one reaction step individually.[31]

$$\text{ALE synergy} = \frac{\text{EPC} - (\alpha + \beta)}{\text{EPC}} \times 100\% \tag{1}$$

The etch per cycle (EPC) is the thickness loss derived from the A/B reaction sequence. The spontaneous etch rates α or β can contribute to etching during the individual A and B reactions, respectively. α and β can be measured as the thickness loss during separate processing with multiple consecutive exposures of one of the reactants alone. The ALE synergy approaches an ideal of 100% when all etching is derived solely from a favorable interaction of the sequential A and B reactions and no etching occurs from either reaction by itself.

This study determined the selectivity by performing thermal ALE and spontaneous etching experiments on SiO_2 and SiN_x under identical reaction conditions. A selectivity factor has been defined to quantify how much a particular process removes the "etch" versus "non-etch" material.[31]

$$\text{selectivity} = \frac{\text{EPC(etch)}}{\text{EPC}'\text{(non-etch)}} \text{ or } \frac{\beta_{\text{HF}}\text{(etch)}}{\beta'_{\text{HF}}\text{(non-etch)}} \tag{2}$$

EPC(etch) and β_{HF}(etch) denote the thickness loss for the "etch" material. Conversely, EPC′(non-etch) and β_{HF}'(non-etch) denote the thickness loss for the "non-etch" material. The selectivity factor approaches an ideal of ∞ when the process removes the "etch" material exclusively and retains all "non-etch" material.

A previous study has achieved selectivity with >10 times faster etching for SiGe thermal ALE compared to Si(100) or Si_3N_4 thermal ALE. This selectivity has been attributed to larger rates for SiGe oxidation and conversion under the same reaction conditions at 290 °C.[24] The present work attempted to develop selectivity between SiO_2 and SiN_x based on differences between the ligand-exchange, conversion, and fluorination reactions during thermal ALE. Other studies have achieved selectivity between SiO_2 and SiN_x using wet or plasma etching approaches.[6,7,12,32,33]

The present work examined the selectivity between SiO_2 and SiN_x for thermal ALE using TMA and HF as the reactants. This study also focused on the spontaneous etching of SiO_2 versus SiN_x using HF alone. In addition, the current work examined selectivity between SiO_2 and SiN_x for a modification of the thermal ALE process using TMA and a codose of HF with ammonia (NH_3). This study further explored the spontaneous etching of SiO_2 versus SiN_x by codosing HF with NH_3.

2. EXPERIMENTAL SECTION

All experiments were conducted at a fixed temperature of 275 °C. This setting was above the transition temperature between thermal atomic layer deposition (ALD) of AlF_3 below 250 °C and thermal ALE of Al_2O_3 above 250 °C.[26,34] 275 °C was also above the thermal desorption temperature of ammonium hexafluorosilicate [$(NH_4)_2SiF_6$] salt that can form during spontaneous etching of both SiN_x and SiO_2.[17,35] In addition, 275 °C was below the decomposition temperature of TMA around 300 °C.[36,37]

2.1. Vacuum Reactor, Reactants, and Thin-Film Samples.

Thermal ALE and spontaneous etching experiments were conducted in a V-shaped, hot-wall, viscous-flow reactor. Detailed descriptions and a computer-aided design cross-section of this apparatus have been published previously.[38,39] A rotary vane pump (Pascal 2010 C1, Pfeiffer Vacuum) evacuated reactants, reaction byproducts, and purge gas. The vacuum system maintained a base pressure in the 10 mTorr range. A capacitance manometer (AA09A11TCE0 Baratron, MKS Instruments) monitored the total pressure in the vacuum chamber. Samples were heated through the hot reactor walls. A temperature controller (2604, Eurotherm) maintained the sample temperature at 275 °C.

Before each etching experiment, the stainless-steel reactor walls and sample holder were coated with ∼10 nm of Al_2O_3 using 100 ALD cycles of TMA (98% purity, Strem) at 1.5 Torr for 15 s and H_2O

(HPLC grade, Fisher Chemical) at 3 Torr for 30 s. Evacuation and purge steps separated the reactant exposures. A linear Al_2O_3 growth of ∼1 Å/cycle was consistent with previous literature benchmarks.[40,41] For a few experiments, designed to obtain better H_2O-free conditions during fluorination, the reactor walls and sample holder were coated with ZrF_4. First, 10 ALD cycles of tetrakis(ethylmethylamino)-zirconium(IV) (TEMAZ, 99% purity, Strem; kept at 110 °C) at 1.5 Torr for 15 s and H_2O at 3 Torr for 30 s deposited a few monolayers of ZrO_2. Then, the ultrathin ZrO_2 ALD film was fluorinated into ZrF_4 using 30 static exposures of HF at 3 Torr for 45 s.[42,43] After the reactor wall coating, a fresh sample was loaded and preheated for 30 min. Thermal ALE alternated between TMA and fluorinating agents for 25 cycles. Spontaneous etching repeated 25 fluorination exposures consecutively.

Anhydrous HF vapor was obtained from a solution of ∼70 wt % HF in ∼30 wt % pyridine (Sigma-Aldrich).[34] TMA and HF-pyridine were kept at room temperature. A codose of HF + NH_3 was derived from heating NH_4F (≥99.99% trace metals basis, Sigma-Aldrich) to 130 °C. Since NH_4F is hygroscopic, absorbed H_2O was thoroughly evacuated by pumping on the heated salt through the reactor.

Every reactant exposure consisted of the following successive steps: first, a 45 s interval evacuated the reactor to base pressure. A closed angular bellows valve then separated the reactor from the pump. Subsequently, the reactant vapor was drawn into the reactor and statically exposed to the sample surface at a total pressure of 3 Torr for 45 s. The open angular bellows valve then reconnected the reactor with the pump for a 15 s evacuation interval plus a 120 s purge step with 150 sccm argon (Ar, ultrahigh purity, Airgas). The reactant sequence, exposure times, and pressures, as well as evacuation and purge steps, were precisely controlled and recorded by a virtual interface programmed in LabVIEW version 19.0.1f5 (National Instruments).

SiO_2 samples were purchased from Silicon Valley Microelectronics. Wet-thermal oxidation was used to grow an initial SiO_2 film thickness of ∼500 nm on single-side-polished, boron-doped ⟨100⟩ Si wafers. SiN_x samples were prepared and provided by Tokyo Electron (TEL). Plasma-enhanced chemical vapor deposition (PE-CVD) was used to deposit an initial SiN_x film thickness of ∼300 nm on 300 mm double-side-polished Si wafers.

The SiN_x film thickness and optical parameters were determined *ex situ* by variable angle spectroscopic ellipsometry (VASE; cf. Supporting Information) with an M-2000 (J.A. Woollam Co.) in the ultraviolet (UV) and visible (VIS) wavelength range from 240 to 1000 nm. One Tauc-Lorentz oscillator, together with a UV pole, sufficiently parametrized the SiN_x layer. The measured refractive index between 2.1 and 2.5 matched the reported value of 2.4 at 248 nm for a Si-rich PE-CVD $SiN_{0.67}$ antireflective coating with ∼22 at. % hydrogen content.[44] In addition, significant observed UV + VIS absorption has been attributed to the formation of Si−Si bonds.[44]

The chemical composition of as-received SiO_2 and SiN_x samples was characterized by X-ray photoelectron spectroscopy (XPS; cf. Supporting Information) in a PHI 5600 system (RBD Instruments) with monochromatic Al K*α* X-ray source (1486.6 eV). XPS spectra were analyzed with CasaXPS software version 2.3.25. XPS confirmed a near stoichiometric composition of SiO_2 and a Si-rich composition of SiN_x with $x \sim 0.8$. Furthermore, the XPS Si 2p peak position and width of SiN_x suggested Si atoms in a chemical environment of both Si−N and Si−Si bonds.

2.2. *In Situ* Spectroscopic Ellipsometry Studies. An *in situ* spectroscopic ellipsometry instrument (iSE, J.A. Woollam Co.) was mounted on the reactor at an angle of incidence of ∼70° to monitor thickness changes during thermal ALE or spontaneous etching. Samples were hand-diced into coupons (0.5 in × 0.5 in), mounted on a horizontal stage with stainless-steel clips, and dusted off with Ar gas. Although the ellipsometer monitored one individual thin film in the reactor at a time, all experiments were conducted under identical conditions. Ellipsometric spectra in the wavelength range from 400 to 1000 nm were acquired after each reactant exposure by integrating over 5 s at the end of the Ar purge step.

The transparent SiO_2 or SiN_x film thicknesses between 100 and 500 nm enabled an interference enhancement.[45] The interference enhancement improved the signal-to-noise ratio toward a confidence interval of ±0.01 Å.[46,47] This confidence interval was determined as the single standard deviation of 30 repeated iSE measurements of the initial film thickness. Thicknesses were shifted to start at zero for each experimental subset. A steady-state etching regime was usually established on each initial pristine surface within five ALE cycles or five consecutive HF or HF + NH_3 exposures. The last 20 of a series of 25 data points were linearly interpolated. The slope of the line determined the corresponding EPC or spontaneous etch rate β. ALE synergy and selectivity factors were calculated according to eqs 1 and 2.

All optical modeling was performed in CompleteEASE software, version 6.57 (J.A. Woollam Co.). SiO_2 samples were modeled as a layer stack of the SiO2_JAW| 10 Å INTR_JAW| Si Temp JAW (275 °C) material files from the CompleteEASE library. SiN_x samples were modeled by stacking a SiN_x layer on top of 25 Å INTR_JAW| Si Temp JAW (275 °C). The optical parameters of this SiN_x layer were extracted from *ex situ* VASE measurements. Surface roughness was included on top of both layer stacks. CompleteEASE modeled this surface roughness as a Bruggeman effective medium approximation layer, mixing 50% of the film material with 50% void. The surface roughness was carefully monitored but usually exhibited no significant change, unless stated otherwise.

3. RESULTS AND DISCUSSION

3.1. SiO_2 Thermal ALE Using TMA/HF and Synergy Factor. Figure 2 shows the changes in SiO_2 layer thickness during the TMA/HF ALE sequence at 275 °C. Each data point represents a single static exposure of 3 Torr for 45 s. The SiO_2 thickness decreased linearly versus the ALE cycle number. The thick solid line linearly interpolates data points after HF exposures, i.e., after complete ALE cycles. This linear fit corresponded to an EPC of 0.20 Å/cycle. The linear thickness loss suggested that sequential TMA and HF exposures effectively removed SiO_2. The EPC was consistent within a range from 0.20 to 0.35 Å/cycle from previous reports for SiO_2 thermal ALE at 300−350 °C.[21,22]

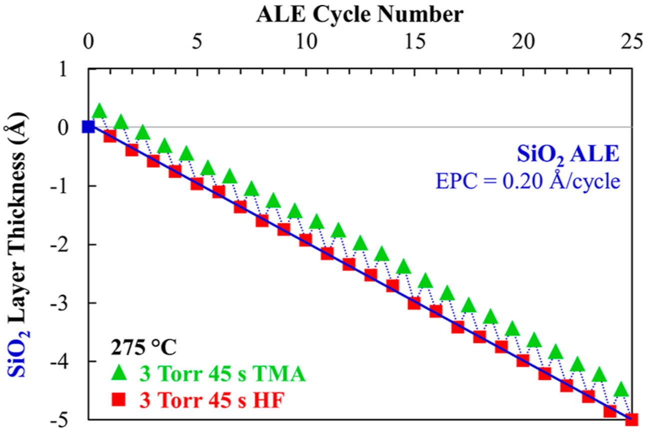

Figure 2. SiO_2 layer thickness vs ALE cycle number for SiO_2 thermal ALE at 275 °C. Each data point represents a single static reactant exposure for TMA or HF of 3 Torr for 45 s. SiO_2 thickness decreased linearly vs ALE cycles with an EPC of 0.20 Å/cycle.

The thickness changes observed in Figure 2 with half-cycle resolution may be understood as convoluted effects on the geometrical thickness or refractive index of the SiO_2 film or its surface.[48] Alkyl groups are highly polarizable as known by their high Raman cross sections.[49,50] Consequently, ellipsometry can sensitively detect their adsorption or removal. During TMA exposures, ligand exchange volatilizes a fluorinated surface layer and converts the underlying SiO_2 film surface. TMA also adsorbs methyl surface species.[21] In this case, the polarizability from adsorbing methyl groups might obscure a thickness loss from the ligand-exchange reaction. During HF exposures, HF removes previously adsorbed surface species and fluorination changes the refractive index of the $AlSi_xO_y$ conversion layer.[21] The effective optical thickness loss after HF exposures may be primarily attributed to the removal of the methyl surface species.

Figure 3 plots the SiO_2 layer thickness during a series of 25 consecutive static exposures of only TMA or HF by themselves, with the same scale as in Figure 2. The first exposure in each series was equivalent to a single TMA or HF exposure during the thermal ALE cycles shown in Figure 2. Consecutive TMA exposures in Figure 3 exhibited a small thickness gain instead of a thickness loss. The TMA half-reaction self-terminated almost entirely within three consecutive exposures. This self-limiting thickness gain was consistent with saturation of the methyl surface coverage. Beyond five exposures, a marginal linear increase continued over 20 exposures at a slope of +0.02 Å per TMA exposure. Since this insignificant increase indicated no undesired etch contribution, α_{TMA} was neglected as zero.

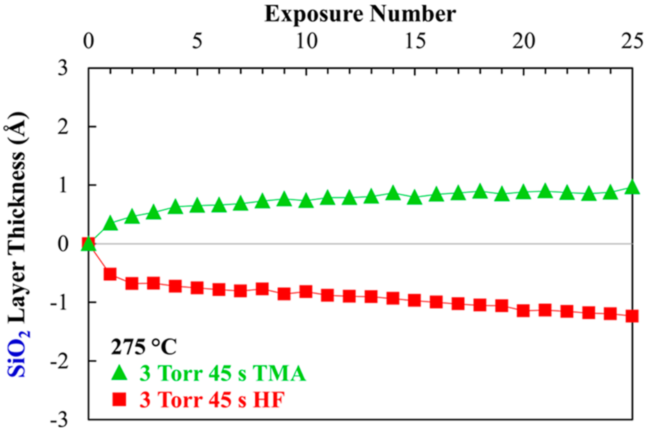

Figure 3. SiO_2 layer thickness vs exposure number of only TMA or HF exposures by themselves. Each individual reactant exposure of TMA or HF was 3 Torr for 45 s. Spontaneous etching of SiO_2 occurred at a rate of 0.02 Å per 45 s HF exposure.

Consecutive HF exposures in Figure 3 exhibited a slight thickness loss. The HF half-reaction self-limited within two consecutive exposures, consistent with effectively removing previously adsorbed methyl groups. Beyond five exposures, a slight thickness decrease continued linearly over 20 exposures with 0.02 Å per 45 s HF exposure. This slight, linear thickness loss signified minor spontaneous etching at $\beta_{HF} = 0.03$ Å/min.

The results in Figure 3 for negligible etching of SiO_2 by HF were consistent with previous studies concluding that anhydrous HF vapor alone cannot etch SiO_2.[21,51,52] However, SiO_2 etching has been observed when H_2O vapor was present together with HF.[53−57] H_2O is believed to facilitate the formation of HF_2^- active etch species from HF that can etch SiO_2 as discussed later in Section 3.1. Consequently, β_{HF} was attributed to a small amount of H_2O that might form during the fluorination of the Al_2O_3 reactor wall coating.[27] Spontaneous etching of SiO_2 would then itself produce more H_2O through the reaction: $SiO_2 + 4HF(g) \rightarrow SiF_4(g) + 2H_2O(g)$.[53−55]

Figures 2 and 3 provide the information needed to evaluate the synergy factor. The linear EPC of 0.20 Å/cycle was considerably greater than a minor, undesired spontaneous etching component of 0.02 Å per HF exposure. A synergy factor of 88% signified that SiO_2 thermal ALE was reasonably ideal at 275 °C. Additional experiments improved this moderate ALE synergy up to 95% by using ZrF_4 as reactor wall passivation instead of an Al_2O_3 ALD coating.[42,43] ZrF_4 passivation leads to better H_2O-free conditions during the HF reaction. ZrF_4 avoids the evolution of H_2O that can occur with Al_2O_3 according to $Al_2O_3 + 6HF(g) \rightarrow 2AlF_3 + 3H_2O(g)$. TMA also removes the AlF_3 surface layer, thereby restoring Al_2O_3 on the walls to release H_2O during every HF exposure. In contrast, ZrF_4 resists reaction with TMA to passivate the reactor walls.[42]

3.2. SiN_x Thermal ALE Using TMA/HF and Synergy Factor. Figure 4 presents the SiN_x layer thickness versus ALE cycle number for thermal ALE using TMA and HF at 275 °C. Each data point represents a single static exposure of 3 Torr for 45 s. The SiN_x thickness decreased linearly versus ALE cycles. The thick solid line linearly interpolates the data points after HF exposures. The linear fit was consistent with an EPC of 1.06 Å/cycle. The significant linear thickness loss suggested that sequential TMA and HF exposures effectively removed SiN_x.

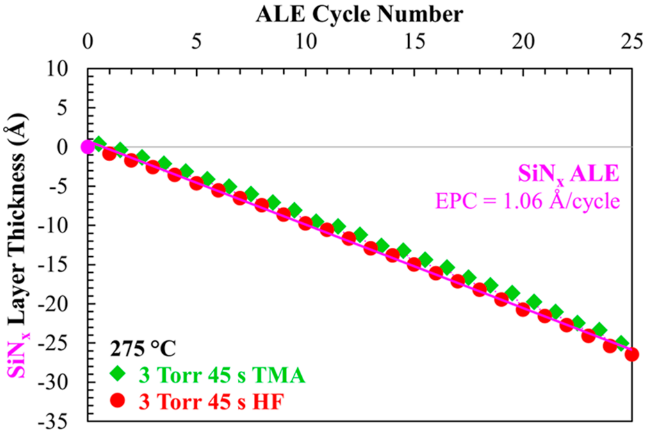

Figure 4. SiN_x layer thickness vs ALE cycle number for SiN_x thermal ALE at 275 °C. Each data point represents a single static reactant exposure for TMA or HF of 3 Torr for 45 s. SiN_x thickness decreased linearly vs ALE cycles with an EPC of 1.06 Å/cycle.

This result for SiN_x thermal ALE was unexpected compared with earlier work that required an oxidation step to obtain Si_3N_4 thermal ALE.[23] The pulse sequence here did not include an oxidation step. HF exposures were 8 Torr·s in the earlier experiments. These HF exposures were significantly lower than the HF exposures of 135 Torr·s in the current studies. In addition, the previously studied Si_3N_4 films were prepared by low-pressure chemical vapor deposition (LP-CVD, University Wafer). The LP-CVD Si_3N_4 was near-stoichiometric with a hydrogen content below 3 at. %. The composition of LP-CVD Si_3N_4 varied substantially from the SiN_x films investigated here that were prepared by PE-CVD. XPS analysis revealed that the PE-CVD SiN_x film was Si-rich with $x \sim 0.8$. In addition, PE-CVD SiN_x probably contained a considerable amount of hydrogen. The contrasting observations between the current

SiN_x ALE experiments and previous Si_3N_4 ALE experiments may be partially attributed to the spontaneous etching of Si-rich SiN_x at higher HF exposures.

Figure 5 plots the SiN_x layer thickness during a series of 25 consecutive static exposures of only TMA or HF by themselves, with the same scale as in Figure 4. The first exposure in each series was equivalent to a single TMA or HF exposure during the ALE cycles shown in Figure 4. Consecutive TMA exposures in Figure 5 exhibited a thickness gain instead of a thickness loss. The TMA half-reaction self-terminated almost entirely within two consecutive exposures, consistent with saturation of the methyl surface coverage. Beyond five exposures, a marginal linear increase continued over 20 exposures at a slope of +0.05 Å per TMA exposure. α_{TMA} was neglected as zero like in Section 3.1.

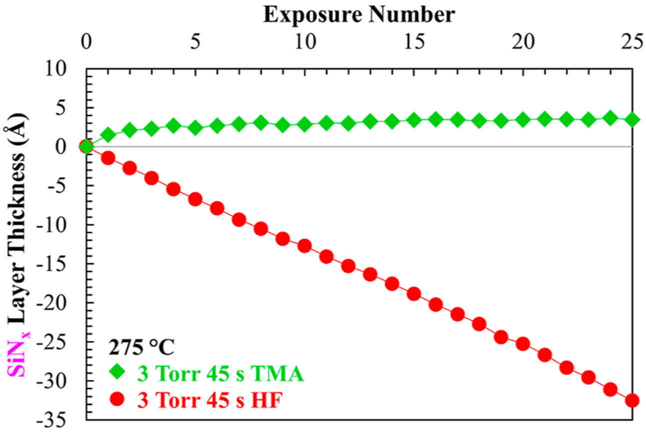

Figure 5. SiN_x layer thickness vs exposure number of only TMA or HF exposures by themselves. Each individual reactant exposure of TMA or HF was 3 Torr for 45 s. Spontaneous etching of SiN_x occurred at a rate of 1.29 Å per 45 s HF exposure.

In contrast, consecutive HF exposures in Figure 5 did not exhibit a self-limiting behavior. The SiN_x thickness decreased linearly during all 25 HF exposures. This continuous linear thickness loss produced a spontaneous etch rate of 1.29 Å per 45 s HF exposure or $\beta_{HF} = 1.72$ Å/min. These results indicated that HF exposures spontaneously etched SiN_x at 275 °C. This major spontaneous etching explained the high EPC for the SiN_x thermal ALE in Figure 4. The spontaneous etching of stoichiometric silicon nitride by HF may occur as $Si_3N_4 + 12HF(g) \rightarrow 3SiF_4(g) + 4NH_3(g)$.

Figures 4 and 5 provide the information needed to evaluate the synergy factor. The spontaneous etching at 1.29 Å per HF exposure was greater than the EPC of 1.06 Å/cycle for SiN_x thermal ALE. Consequently, eq 1 calculated a synergy factor of −22%. This negative value indicated that SiN_x spontaneous etching predominated over the ALE sequence when anhydrous HF vapor was used at 275 °C.

3.3. Selectivity between Al_2O_3, SiO_2, and SiN_x Thermal ALE Using TMA/HF.

Figure 6 compares SiO_2 and SiN_x thermal ALE with sequential TMA and HF exposures of 3 Torr for 45 s at 275 °C. These results were shown earlier in Figures 2 and 4. Figure 6 also includes results for the thermal ALE of an Al_2O_3 ALD film at 275 °C for comparison. Al_2O_3 thermal ALE using TMA and HF as the reactants is included because this system is the model thermal ALE process.[25,30,58] Each sample was monitored individually but under identical process conditions. The Al_2O_3, SiO_2, and SiN_x film thicknesses all decreased linearly with ALE cycles.

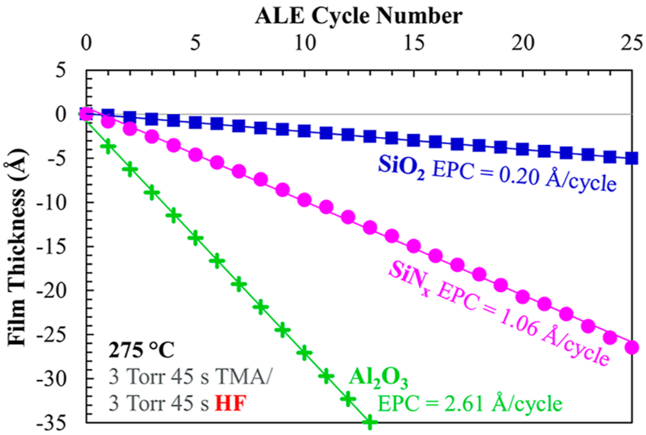

Figure 6. Film thickness vs ALE cycle number for SiO_2, SiN_x, and Al_2O_3 thermal ALE using TMA and HF exposures at 275 °C. EPCs were 2.61, 1.06, and 0.20 Å/cycle for Al_2O_3, SiN_x, and SiO_2, respectively. Selectivity factor was ∼5:1 for SiN_x etching compared to SiO_2 etching (preferential SiN_x removal).

Figure 6 reveals that the slopes of the linear thickness losses versus the ALE cycle number were different for each material. The EPCs were 2.61, 1.06, and 0.20 Å/cycle for Al_2O_3, SiN_x, and SiO_2, respectively. The EPC for Al_2O_3 thermal ALE was consistent with previous reports ranging from 0.14 to 2.50 Å/cycle at reactant pressures from 40 mTorr to 5 Torr and temperatures between 250 and 300 °C.[25,30,58,59] The EPC for SiO_2 thermal ALE was also consistent with previous works.[21,22] The EPC for SiN_x thermal ALE was much larger than in previous work for Si_3N_4 thermal ALE at lower HF exposures.[23]

Equation 2 was used to determine a moderate selectivity factor of ∼5:1 for preferential etching of SiN_x compared to SiO_2. However, SiN_x thermal ALE exhibited no synergy because the spontaneous etching of SiN_x during HF exposures was not self-limiting. Larger HF exposures would continue to increase the selectivity factor because the HF exposure during SiN_x thermal ALE is not self-limiting.

3.4. Selectivity between SiO_2 and SiN_x Spontaneous Etching Using HF Alone.

Figure 7 shows the film thickness versus HF exposure number to compare the selectivity between SiO_2 and SiN_x for spontaneous etching using only HF exposures. Each sample was monitored individually under identical process conditions for a series of 25 consecutive static HF exposures at 3 Torr for 45 s. These results were shown earlier in Figures 3 and 5. The SiO_2 film thickness decreased slightly with consecutive HF exposures at an etch rate of 0.03 Å/min. This negligible SiO_2 etching was consistent with previous literature.[21,51,52] In contrast, the SiN_x film thickness decreased linearly with consecutive HF exposures at an etch rate of 1.72 Å/min. The spontaneous etch rate of SiN_x was much larger than the spontaneous etch rate of SiO_2.

Equation 2 calculated a significantly higher selectivity factor of ∼50:1 for SiN_x etching compared to SiO_2 etching. Larger HF exposures continued to increase the selectivity factor to ∼150:1 at 9 Torr. Ensuring H_2O-free conditions during HF exposures may improve this high selectivity even further. A literature report for wet etching employing an organic solution with 10 mass % anhydrous HF at 80 °C has shown that selectivity for spontaneous etching of SiN_x over SiO_2 was highest at 15:1 under H_2O-free conditions.[52]

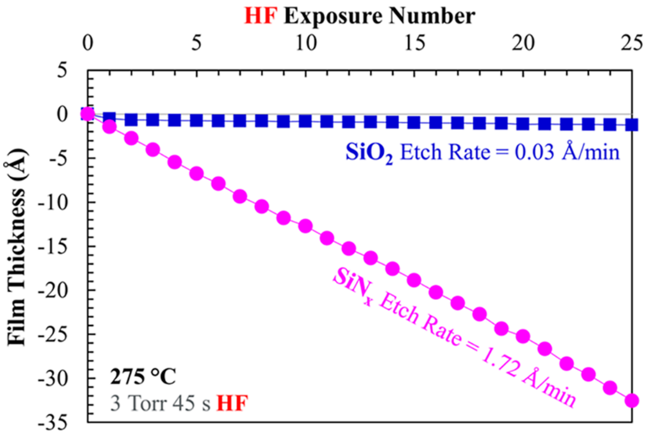

Figure 7. Film thickness vs HF exposure number comparing SiO_2 and SiN_x spontaneous etching using HF alone at 275 °C. Etch rates were 1.72 Å/min for SiN_x and 0.03 Å/min for SiO_2. Selectivity factor was ~50:1 for SiN_x etching compared to SiO_2 etching (preferential SiN_x removal) at 3 Torr HF pressure.

3.5. SiO_2 Thermal ALE Using TMA/HF + NH_3 Codosing and Synergy Factor.

The effect of NH_3 codosing during the HF exposures was examined to determine if coadsorbates could change the nature of the active etch species and influence the ALE synergy and selectivity. Figure 8a displays the changes in the SiO_2 layer thickness during the thermal ALE sequence that cycled between separate exposures of TMA and HF + NH_3 codosing at 275 °C. HF + NH_3 codosing was obtained from evaporating NH_4F salt at 130 °C. Each single static exposure was 3 Torr for 45 s. The SiO_2 thickness decreased substantially versus the ALE cycle number. A thickness loss of 132.44 Å was measured after 15 ALE cycles. Dividing this thickness loss by 15 ALE cycles yields an average EPC of 8.83 Å/cycle. In addition, the SiO_2 surface roughness increased noticeably with every ALE cycle. The large EPC with significant surface roughening suggested that rapid spontaneous etching of SiO_2 occurred during this SiO_2 thermal ALE process with HF + NH_3 codosing.

To check for spontaneous etching, a SiO_2 film was examined under the same HF + NH_3 codosing conditions as employed in Figure 8a. Figure 8b shows the SiO_2 layer thickness during a series of 25 consecutive static HF + NH_3 codosing exposures, with the same scale as Figure 8a. The large thickness decrease continued beyond the eight HF + NH_3 exposures shown in Figure 8b. The thickness loss was 515.61 Å after 25 consecutive HF + NH_3 exposures. Dividing this thickness loss by 25 exposures yields an average etch rate of 20.62 Å per 45 s HF + NH_3 exposure or β_{HF+NH_3} = 27.50 Å/min.

Codosing HF + NH_3 opened a new pathway for rapid spontaneous etching of SiO_2 compared to exposing HF vapor by itself without NH_3 codosing. The spontaneous etching component at 20.62 Å per HF + NH_3 exposure was greater than the EPC of 8.83 Å/cycle during SiO_2 thermal ALE with HF + NH_3 codosing. These results indicated that TMA exposures slowed the rapid SiO_2 spontaneous etching during the HF + NH_3 codosing. Equation 1 calculated a synergy factor of −134% for SiO_2 thermal ALE with HF + NH_3 codosing. This negative value indicated that rapid spontaneous etching of SiO_2 predominated over the ALE sequence when codosing HF + NH_3 at 275 °C.

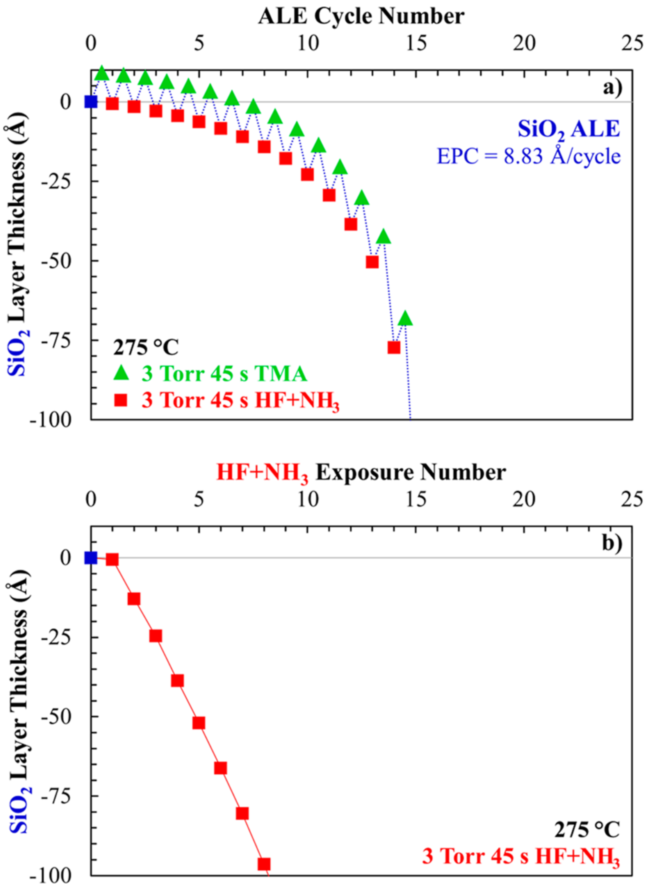

Figure 8. (a) SiO_2 layer thickness vs ALE cycle number for SiO_2 thermal ALE using TMA and HF + NH_3 codosing at 275 °C. Each data point represents a single static reactant exposure for TMA or HF + NH_3 of 3 Torr for 45 s. SiO_2 thickness decreased vs ALE cycles with an EPC of 8.83 Å/cycle averaged over 15 ALE cycles. (b) SiO_2 layer thickness vs HF + NH_3 exposure number. Each HF + NH_3 exposure was 3 Torr for 45 s. Spontaneous etching of SiO_2 occurred at a rate of 20.62 Å per 45 s HF + NH_3 exposure.

3.6. SiN_x Thermal ALE Using TMA/HF + NH_3 Codosing and Synergy Factor.

The effect of NH_3 codosing during HF exposures was also examined on SiN_x films. Figure 9a displays the changes in the SiN_x layer thickness during the TMA/HF + NH_3 ALE sequence at 275 °C. Each single static exposure was 3 Torr for 45 s. The SiN_x thickness remained virtually constant versus the ALE cycle number. The thick solid line linearly interpolates data points after HF + NH_3 exposures, i.e., after complete ALE cycles. This linear fit was consistent with an EPC smaller than the confidence interval of ±0.01 Å/cycle. The thickness retention indicated that sequential TMA and HF + NH_3 exposures cannot etch SiN_x. The oscillations in the SiN_x layer thickness were attributed to surface methyl groups being added by TMA and removed by HF exposures.

Figure 9b explores the possibility for spontaneous etching of SiN_x by 25 consecutive static exposures of HF + NH_3 codosing. The first exposure in this series was equivalent to a single HF + NH_3 exposure during the SiN_x thermal ALE shown in Figure 9a. Consecutive HF + NH_3 exposures in Figure 9b exhibited a marginal thickness decrease with a spontaneous etch rate of 0.01 Å per 45 s HF + NH_3 exposure or β_{HF+NH_3} = 0.02 Å/min. Codosing HF + NH_3 dramatically stopped the spontaneous etching of SiN_x compared to the large spontaneous etch rate β_{HF} monitored in Figure 5 when using HF exposures without NH_3.

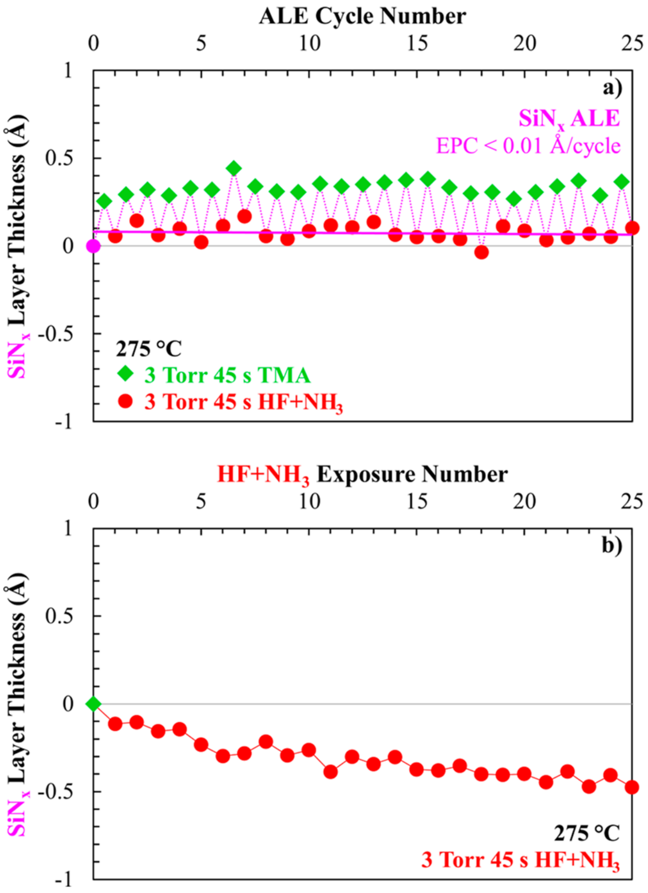

Figure 9. (a) SiN$_x$ layer thickness vs ALE cycle number for SiN$_x$ thermal ALE using TMA and HF + NH$_3$ codosing at 275 °C. Each data point represents a single static reactant exposure for TMA or HF + NH$_3$ of 3 Torr for 45 s. SiN$_x$ thickness remained virtually constant vs ALE cycles. (b) SiN$_x$ layer thickness vs HF + NH$_3$ exposure number. Each HF + NH$_3$ exposure was 3 Torr for 45 s. Spontaneous etching of SiN$_x$ occurred at a rate of 0.01 Å per 45 s HF + NH$_3$ exposure.

Both the negligible EPC and $\beta_{\mathrm{HF+NH_3}}$ indicated that codosing HF + NH$_3$ dramatically restricted the spontaneous etching of SiN$_x$ compared to the large SiN$_x$ removal observed using HF exposures without NH$_3$ in Figure 5. SiN$_x$ resisted thermal ALE and spontaneous etching when codosing HF + NH$_3$. Therefore, calculating a synergy factor was not meaningful. SiN$_x$ had no direct etch pathway through conversion, fluorination, and ligand exchange when HF + NH$_3$ codosing restricted the spontaneous etching of SiN$_x$.

3.7. Selectivity between SiO$_2$ and SiN$_x$ Thermal ALE Using TMA/HF + NH$_3$ Codosing. Given that SiN$_x$ thermal ALE and SiN$_x$ spontaneous etching were both negligible with HF + NH$_3$ codosing, the selectivity between SiO$_2$ and SiN$_x$ was expected to be high. Figure 10 directly compares the SiO$_2$ and SiN$_x$ film thicknesses versus the ALE cycle number. The EPC was 8.83 Å/cycle for SiO$_2$ thermal ALE with HF + NH$_3$ codosing from Figure 8a. In contrast, the EPC remained below the confidence limit of ±0.01 Å/cycle for SiN$_x$ thermal ALE with HF + NH$_3$ codosing from Figure 9a.

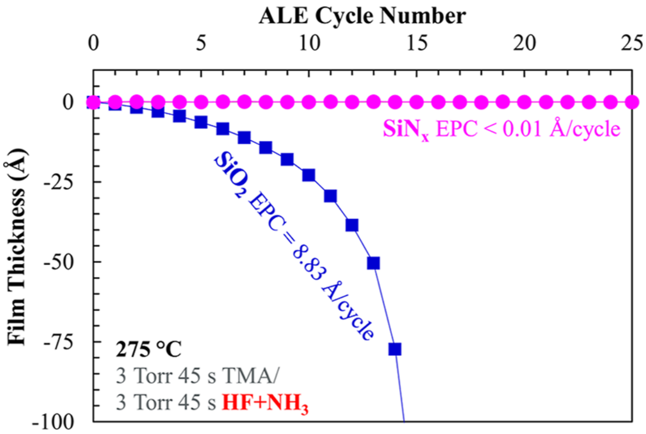

Figure 10. Comparison between SiO$_2$ and SiN$_x$ film thickness vs ALE cycle number for thermal ALE using TMA and HF + NH$_3$ codosing at 275 °C. EPCs were 8.83 Å/cycle for SiO$_2$ and <0.01 Å/cycle for SiN$_x$. Selectivity factor was >1000:1 for SiO$_2$ etching compared to SiN$_x$ etching (preferential SiO$_2$ removal).

Based on the results in Figure 10, eq 2 calculated an exceptionally high selectivity factor >1000:1 for SiO$_2$ etching compared to SiN$_x$ etching for thermal ALE using sequential exposures of TMA and HF + NH$_3$ codosing. This exceptional selectivity for preferential SiO$_2$ removal with HF + NH$_3$ codosing was reversed compared to the ∼5:1 selectivity for preferential SiN$_x$ removal observed in Figure 6 without NH$_3$ codosing.

3.8. Selectivity between SiO$_2$ and SiN$_x$ Spontaneous Etching Codosing HF + NH$_3$. Figure 11 shows the selectivity between SiO$_2$ and SiN$_x$ for spontaneous etching using HF + NH$_3$ codosing. The etch rate was 27.50 Å/min for SiO$_2$ spontaneous etching with HF + NH$_3$ codosing, partially from Figure 8b. In contrast, the etch rate of 0.02 Å/min was negligible for SiN$_x$ spontaneous etching with HF + NH$_3$ codosing from Figure 9b.

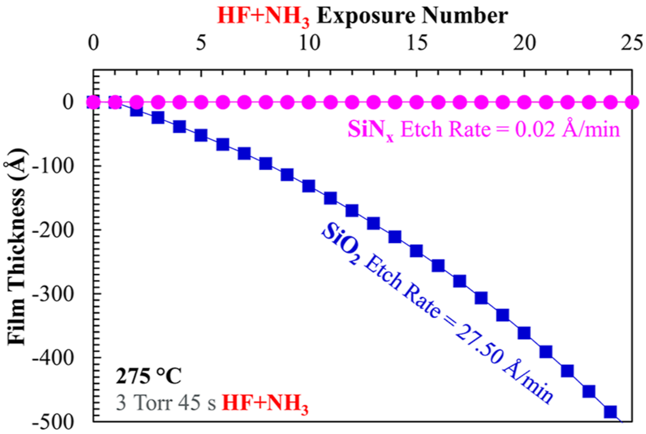

Figure 11. Comparison between SiO$_2$ and SiN$_x$ film thickness vs HF + NH$_3$ exposure number for spontaneous etching at 275 °C. Etch rates were 27.50 Å/min for SiO$_2$ and 0.02 Å/min for SiN$_x$. Selectivity factor was >1000:1 for SiO$_2$ etching compared to SiN$_x$ etching (preferential SiO$_2$ removal).

Based on these dramatically different etch rates, eq 2 calculated a high selectivity factor of >1000:1 for SiO$_2$ spontaneous etching compared to SiN$_x$ spontaneous etching using HF + NH$_3$ codosing. This exceptional selectivity for preferential SiO$_2$ removal with HF + NH$_3$ codosing was reversed compared to the selectivity for preferential SiN$_x$ removal observed in Figure 7 without NH$_3$ codosing. These

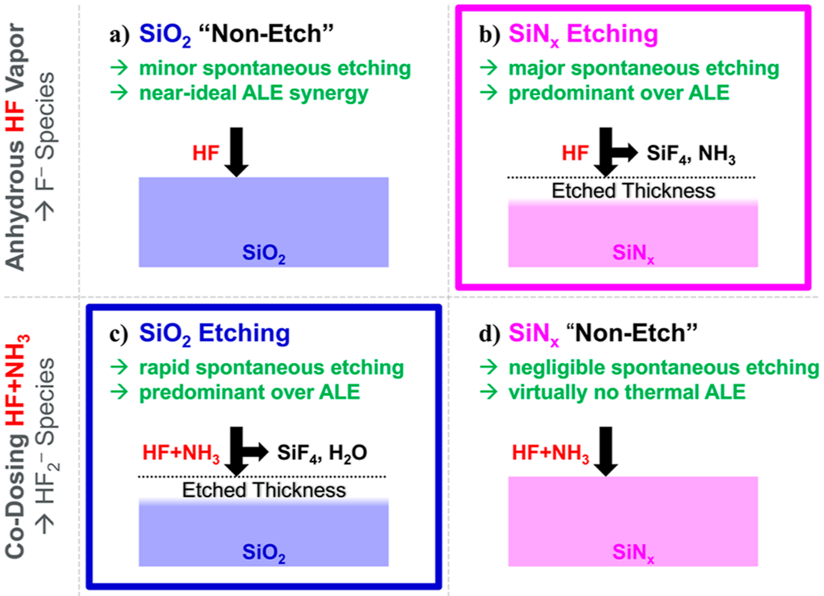

Figure 12. Spontaneous etching scenarios for SiO_2 and SiN_x using HF exposures or HF + NH_3 codosing exposures. (a) No etching of SiO_2 for HF exposures and near-ideal ALE synergy. (b) Major spontaneous etching of SiN_x for HF exposures and no ALE synergy. (c) Rapid spontaneous etching of SiO_2 for HF + NH_3 codosing exposures and no ALE synergy. (d) No etching of SiN_x for HF + NH_3 codosing exposures.

results illustrated that the NH_3 coadsorbate played a key role in dictating etch selectivity.

3.9. Etch Species during HF Exposures and HF + NH_3 Codosing Exposures. Figure 12 summarizes all of the spontaneous etching scenarios explored in this paper. The top row addresses anhydrous HF vapor alone. Figure 12a illustrates SiO_2 "non-etch" by HF, resulting in near ideal synergy for SiO_2 thermal ALE using TMA and HF. In contrast, Figure 12b highlights the major SiN_x spontaneous etching by HF, predominating over the respective ALE sequence. The bottom row addresses HF + NH_3 codosing. Figure 12c highlights the rapid SiO_2 spontaneous etching by HF + NH_3, predominating over the respective ALE sequence. Figure 12d illustrates the SiN_x "non-etch" by HF + NH_3, resulting in virtually no SiN_x thermal ALE using TMA and HF + NH_3, as well as negligible SiN_x spontaneous etching using HF + NH_3 codosing.

The SiO_2 and SiN_x etching results differed substantially, depending on whether HF was used alone or codosed with NH_3. These systematic differences may be explained by the nature of the active etch species. Literature studies for aqueous HF solutions have established that SiO_2 wet etching is mainly determined by HF_2^- species.[60,61] SiO_2 nonetch has also been reported for anhydrous, un-ionized HF.[21,51,52] Likewise, studies for aqueous HF solutions have established that SiN_x wet etching is largely determined by F^- species. The same studies have reported that un-ionized HF can etch SiN_x at a lower reaction rate and HF_2^- species cannot etch SiN_x.[44,61] These results from wet, solution etching can provide guidance to understand the active etch species present during dry, gas-phase HF exposures and HF + NH_3 codosing exposures.

During HF exposures at 3 Torr, HF may partially dissociate into H^+ and F^- in the adsorbed HF layer on the surface. An adsorbed HF layer may be needed to solvate the H^+ and F^- ions formed after HF dissociation. Other investigations have documented an adsorbed HF layer with hydrogen-bonding between the HF adsorbates on Al_2O_3 surfaces.[26,34] HF dissociation in the adsorbed HF layer may not be extensive, and most of the dissociation products may remain as F^- without continuing to form HF_2^-. These conditions would favor SiN_x etching based on the previous aqueous HF solution studies.[44,61]

In contrast, during HF + NH_3 codosing exposures at 3 Torr, HF dissociation may be more extensive. NH_3 may help stabilize the H^+ dissociation product and lead to higher concentrations of the F^- dissociation product. At the increased F^- concentrations, the reaction of F^- with HF may produce HF_2^- species. These conditions would favor SiO_2 etching based on previous aqueous HF solution studies.[60,61]

H_2O is believed to have a similar effect on HF. An adsorbed H_2O layer can solvate H^+ and F^- ions formed after HF dissociation. The formation of HF_2^- species then promotes SiO_2 etching.[60,61] Consequently, the presence of H_2O can decrease the selectivity of SiN_x etching compared to SiO_2 etching by increasing the SiO_2 etch rate. The vapor-phase SiO_2 etching with HF + methanol or HF + ethanol codosing also suggests a similar role for alcohols. The alcohol is believed to facilitate HF dissociation and promote the formation of HF_2^- species for SiO_2 etching.[62−66]

As an alternative explanation, earlier work has shown that NH_3 as an amine can catalyze reactions with hydroxyl groups on SiO_2.[38,67−69] Si−OH surface species have a very acidic hydrogen with an isoelectric point at a pH level around two.[70] Amine coupling to this acidic hydrogen makes oxygen in the Si−OH surface species a much stronger nucleophile. As a result, NH_3 might catalyze the reaction of HF with Si−OH surface species to produce gaseous H_2O and Si−F surface species. In contrast, NH_3 is not expected to interact in the same way with the Si−NH_2 surface species on SiN_x films.

4. CONCLUSIONS

This study explored the selectivity between SiO_2 and SiN_x thermal ALE using TMA and HF as the reactants at 275 °C. An EPC of 0.20 Å/cycle was measured for SiO_2 thermal ALE using sequential TMA and HF with reactant exposures of 3 Torr for 45 s. A negligible spontaneous etching of SiO_2 at the same HF exposures of 3 Torr for 45 s determined that SiO_2 thermal ALE had near-ideal synergy up to 95%.

In contrast, SiN_x thermal ALE performed under the same reaction conditions as SiO_2 thermal ALE observed a higher EPC of 1.06 Å/cycle. These results were surprising because SiN_x thermal ALE did not include an oxidation reaction. The SiN_x thermal ALE results suggested that HF exposures alone can etch SiN_x spontaneously. Measurements employing multiple consecutive HF exposures confirmed significant SiN_x spontaneous etching by anhydrous HF vapor. This spontaneous etching of SiN_x led to no synergy for SiN_x thermal ALE. SiN_x spontaneous etching by HF itself was greater than the etching during SiN_x thermal ALE.

In addition, the selectivity factor was ~5:1 for SiN_x etching compared to SiO_2 etching (preferential SiN_x removal) during the thermal ALE process. The selectivity factor was higher for spontaneous etching using HF exposures alone. The spontaneous etch rates were 1.72 Å/min for SiN_x etching compared to 0.03 Å/min for SiO_2 etching. The selectivity factor was ~50:1 for SiN_x spontaneous etching compared to SiO_2 spontaneous etching at 3 Torr. The selective SiN_x etching was attributed to F^- species present during HF pressures at 3 Torr. F^- is the active species for SiN_x etching according to previous solution studies.

NH_3 as a coadsorbate during HF exposures was determined to have a dramatic effect on the thermal ALE and spontaneous etching at 275 °C. SiO_2 and SiN_x thermal ALE were explored with sequential TMA and HF + NH_3 codosing exposures of 3 Torr for 45 s. A much higher EPC of 8.83 Å/cycle was measured during SiO_2 thermal ALE with HF + NH_3 codosing. The spontaneous etching of SiO_2 with HF + NH_3 codosing exposures yielded an even higher etch rate of 27.50 Å/min. In contrast, the EPC was negligible for SiN_x thermal ALE with HF + NH_3 codosing. The spontaneous etching of SiN_x with HF + NH_3 codosing exposures also produced a negligible etch rate.

A high selectivity factor of >1000:1 for SiO_2 etching compared to SiN_x etching (preferential SiO_2 removal) was determined during thermal ALE with HF + NH_3 codosing. Likewise, a high selectivity factor of >1000:1 for SiO_2 etching compared to SiN_x etching was measured during spontaneous etching with HF + NH_3 codosing. The selective SiO_2 etching was attributed to HF_2^- species present during HF + NH_3 codosing exposures at 3 Torr. NH_3 may promote the dissociation of HF into H^+ and F^-. The increased F^- concentration then may produce HF_2^- species. HF_2^- is the active species for SiO_2 etching based on solution studies.

This comparison of HF exposures and HF + NH_3 codosing exposures illustrated that the presence of NH_3 coadsorbates can modify the active species during vapor-phase HF etching. The change in active species from F^- with HF exposures to HF_2^- with HF + NH_3 codosing exposures altered the etch selectivity from SiN_x to SiO_2. This reciprocal etch selectivity may be employed for the selective removal of sacrificial SiO_2 or SiN_x in composite structures.

ASSOCIATED CONTENT

Supporting Information

The Supporting Information is available free of charge at https://pubs.acs.org/doi/10.1021/acs.chemmater.4c01040.

Characterization of initial SiO_2 and PE-CVD SiN_x thin-film samples utilizing VASE and XPS (PDF)

AUTHOR INFORMATION

Corresponding Author

Marcel Junige − *Department of Chemistry, University of Colorado, Boulder, Colorado 80309-0215, United States;* orcid.org/0000-0002-6633-2759; Email: marcel.junige@colorado.edu

Author

Steven M. George − *Department of Chemistry, University of Colorado, Boulder, Colorado 80309-0215, United States;* orcid.org/0000-0003-0253-9184

Complete contact information is available at: https://pubs.acs.org/10.1021/acs.chemmater.4c01040

Notes

The authors declare no competing financial interest.

ACKNOWLEDGMENTS

The Semiconductor Research Corporation (SRC) funded this work (NMP Task ID 3083.001). The authors thank Andrew S. Cavanagh for XPS measurements. Tokyo Electron (TEL) provided the SiN_x samples. The authors also thank all their SRC liaisons for this project, especially Scott Clendenning, Tristan A. Tronic, Dominique Adams (Intel); Hanna Paddubrouskaya, Kanda Tapily (TEL); Dominik Metzler (IBM); Petro Deminskyi, Glen Wilk (ASM); and Harsono Simka (Samsung) for their valuable feedback.

REFERENCES

(1) Chen, Y.; Shu, Z.; Zhang, S.; Zeng, P.; Liang, H.; Zheng, M.; Duan, H. Sub-10 nm Fabrication: Methods and Applications. *Int. J. Extreme Manuf.* **2021**, *3*, 032002.

(2) Mulkens, J.; Hanna, M.; Slachter, B.; Tel, W.; Kubis, M.; Maslow, M.; Spence, C.; Timoshkov, V. Patterning Control Strategies for Minimum Edge Placement Error in Logic Devices. *Proc. SPIE* **2017**, *10145*, 1014505.

(3) Mackus, A. J. M.; Merkx, M. J. M.; Kessels, W. M. M. From the Bottom-Up: Toward Area-Selective Atomic Layer Deposition with High Selectivity. *Chem. Mater.* **2019**, *31*, 2−12.

(4) Parsons, G. N.; Clark, R. D. Area-Selective Deposition: Fundamentals, Applications, and Future Outlook. *Chem. Mater.* **2020**, *32*, 4920−4953.

(5) Carver, C. T.; Plombon, J. J.; Romero, P. E.; Suri, S.; Tronic, T. A.; Turkot, R. B., Jr. Atomic Layer Etching: An Industry Perspective. *ECS J. Solid State Sci. Technol.* **2015**, *4*, N5005−N5009.

(6) Kim, T.; Park, T.; Lim, S. Improvement of Si_3N_4/SiO_2 Etching Selectivity through the Passivation of SiO_2 Surface in Aromatic Carboxylic Acid-Added H_3PO_4 Solutions for the 3D NAND Integration. *Appl. Surf. Sci.* **2023**, *619*, 156758.

(7) Lee, H. I.; Kim, H. S.; Tikue, E. T.; Kang, S. K.; Zhang, H.; Park, J. W.; Yang, S.; Lee, P. S. Green Manufacturing of Silyl-Phosphate for Use in 3D NAND Flash Memory Fabrication. *ACS Sustainable Chem. Eng.* **2021**, *9*, 4948−4956.

(8) Chini, S. F.; Amirfazli, A. Understanding Pattern Collapse in Photolithography Process Due to Capillary Forces. *Langmuir* **2010**, *26*, 13707−13714.

(9) Oehrlein, G. S. Reactive-Ion Etching. *Phys. Today* **1986**, *39*, 26−33.

(10) Oehrlein, G. S.; Metzler, D.; Li, C. Atomic Layer Etching at the Tipping Point: An Overview. *ECS J. Solid State Sci. Technol.* **2015**, *4*, N5041−N5053.

(11) Khan, S. A.; Suyatin, D. B.; Sundqvist, J.; Graczyk, M.; Junige, M.; Kauppinen, C.; Kvennefors, A.; Huffman, M.; Maximov, I. High-Definition Nanoimprint Stamp Fabrication by Atomic Layer Etching. *ACS Appl. Nano Mater.* **2018**, *1*, 2476−2482.

(12) Gasvoda, R. J.; Zhang, Z.; Wang, S.; Hudson, E. A.; Agarwal, S. Etch Selectivity During Plasma-Assisted Etching of SiO_2 and SiN_x: Transitioning from Reactive Ion Etching to Atomic Layer Etching. *J. Vac. Sci. Technol. A* **2020**, *38*, 050803.

(13) Tinacba, E. J. C.; Isobe, M.; Hamaguchi, S. Surface Damage Formation During Atomic Layer Etching of Silicon with Chlorine Adsorption. *J. Vac. Sci. Technol. A* **2021**, *39*, 042603.

(14) Yabumoto, N.; Oshima, M.; Michikami, O.; Yoshii, S. Surface Damage on Si Substrates Caused by Reactive Sputter Etching. *Jpn. J. Appl. Phys.* **1981**, *20*, 893−900.

(15) George, S. M.; Lee, Y. Prospects for Thermal Atomic Layer Etching Using Sequential, Self-Limiting Fluorination and Ligand-Exchange Reactions. *ACS Nano* **2016**, *10*, 4889−4894.

(16) Fischer, A.; Routzahn, A.; George, S. M.; Lill, T. Thermal Atomic Layer Etching: A Review. *J. Vac. Sci. Technol. A* **2021**, *39*, 030801.

(17) Ohtake, H.; Miyoshi, N.; Shinoda, K.; Fujisaki, S.; Yamaguchi, Y. Isotropic Atomic Layer Etchings of Various Materials by Using Dry Chemical Removal. *Jpn. J. Appl. Phys.* **2023**, *62*, SG0801.

(18) Kanarik, K. J.; Lill, T.; Hudson, E. A.; Sriraman, S.; Tan, S.; Marks, J.; Vahedi, V.; Gottscho, R. A. Overview of Atomic Layer Etching in the Semiconductor Industry. *J. Vac. Sci. Technol. A* **2015**, *33*, 020802.

(19) George, S. M. Mechanisms of Thermal Atomic Layer Etching. *Acc. Chem. Res.* **2020**, *53*, 1151−1160.

(20) Abdulagatov, A. I.; George, S. M. Thermal Atomic Layer Etching of Silicon Using O_2, HF, and $Al(CH_3)_3$ as the Reactants. *Chem. Mater.* **2018**, *30*, 8465−8475.

(21) DuMont, J. W.; Marquardt, A. E.; Cano, A. M.; George, S. M. Thermal Atomic Layer Etching of SiO_2 by a "Conversion-Etch" Mechanism Using Sequential Reactions of Trimethylaluminum and Hydrogen Fluoride. *ACS Appl. Mater. Interfaces* **2017**, *9*, 10296−10307.

(22) Rahman, R.; Mattson, E. C.; Klesko, J. P.; Dangerfield, A.; Rivillon-Amy, S.; Smith, D. C.; Hausmann, D.; Chabal, Y. J. Thermal Atomic Layer Etching of Silica and Alumina Thin Films Using Trimethylaluminum with Hydrogen Fluoride or Fluoroform. *ACS Appl. Mater. Interfaces* **2018**, *10*, 31784−31794.

(23) Abdulagatov, A. I.; George, S. M. Thermal Atomic Layer Etching of Silicon Nitride Using an Oxidation and "Conversion Etch" Mechanism. *J. Vac. Sci. Technol. A* **2020**, *38*, 022607.

(24) Abdulagatov, A. I.; Sharma, V.; Murdzek, J. A.; Cavanagh, A. S.; George, S. M. Thermal Atomic Layer Etching of Germanium-Rich SiGe Using an Oxidation and "Conversion-Etch" Mechanism. *J. Vac. Sci. Technol. A* **2021**, *39*, 022602.

(25) Lee, Y.; DuMont, J. W.; George, S. M. Trimethylaluminum as the Metal Precursor for the Atomic Layer Etching of Al_2O_3 Using Sequential, Self-Limiting Thermal Reactions. *Chem. Mater.* **2016**, *28*, 2994−3003.

(26) DuMont, J. W.; George, S. M. Competition between Al_2O_3 Atomic Layer Etching and AlF_3 Atomic Layer Deposition Using Sequential Exposures of Trimethylaluminum and Hydrogen Fluoride. *J. Chem. Phys.* **2017**, *146*, 052819.

(27) Clancey, J. W.; Cavanagh, A. S.; Smith, J. E. T.; Sharma, S.; George, S. M. Volatile Etch Species Produced During Thermal Al_2O_3 Atomic Layer Etching. *J. Phys. Chem. C* **2020**, *124*, 287−299.

(28) Lii-Rosales, A.; Cavanagh, A. S.; Fischer, A.; Lill, T.; George, S. M. Spontaneous Etching of Metal Fluorides Using Ligand-Exchange Reactions: Landscape Revealed by Mass Spectrometry. *Chem. Mater.* **2021**, *33*, 7719−7730.

(29) Lee, Y.; Huffman, C.; George, S. M. Selectivity in Thermal Atomic Layer Etching Using Sequential, Self-Limiting Fluorination and Ligand-Exchange Reactions. *Chem. Mater.* **2016**, *28*, 7657−7665.

(30) Cano, A. M.; Marquardt, A. E.; DuMont, J. W.; George, S. M. Effect of HF Pressure on Thermal Al_2O_3 Atomic Layer Etch Rates and Al_2O_3 Fluorination. *J. Phys. Chem. C* **2019**, *123*, 10346−10355.

(31) Kanarik, K. J.; Tan, S.; Gottscho, R. A. Atomic Layer Etching: Rethinking the Art of Etch. *J. Phys. Chem. Lett.* **2018**, *9*, 4814−4821.

(32) Kastenmeier, B. E. E.; Matsuo, P. J.; Oehrlein, G. S. Highly Selective Etching of Silicon Nitride over Silicon and Silicon Dioxide. *J. Vac. Sci. Technol. A* **1999**, *17*, 3179−3184.

(33) Seo, D.; Bae, J. S.; Oh, E.; Kim, S.; Lim, S. Selective Wet Etching of Si_3N_4/SiO_2 in Phosphoric Acid with the Addition of Fluoride and Silicic Compounds. *Microelectron. Eng.* **2014**, *118*, 66−71.

(34) Lee, Y.; DuMont, J. W.; Cavanagh, A. S.; George, S. M. Atomic Layer Deposition of AlF_3 Using Trimethylaluminum and Hydrogen Fluoride. *J. Phys. Chem. C* **2015**, *119*, 14185−14194.

(35) Miyoshi, N.; Kobayashi, H.; Shinoda, K.; Kurihara, M.; Watanabe, T.; Kouzuma, Y.; Yokogawa, K.; Sakai, S.; Izawa, M. Atomic Layer Etching of Silicon Nitride Using Infrared Annealing for Short Desorption Time of Ammonium Fluorosilicate. *Jpn. J. Appl. Phys.* **2017**, *56*, 06HB01.

(36) Yeddanapalli, L. M.; Schubert, C. C. Thermal and Photochemical Decomposition of Gaseous Aluminum Trimethyl. *J. Chem. Phys.* **1946**, *14*, 1−7.

(37) Puurunen, R. L.; Lindblad, M.; Root, A.; Krause, A. O. I. Successive Reactions of Gaseous Trimethylaluminium and Ammonia on Porous Alumina. *Phys. Chem. Chem. Phys.* **2001**, *3*, 1093−1102.

(38) Junige, M.; George, S. M. Area-Selective Molecular Layer Deposition of Nylon 6,2 Polyamide: Growth on Carbon and Inhibition on Silica. *J. Vac. Sci. Technol. A* **2021**, *39*, 023204.

(39) Collings, M. A.; Junige, M.; Cavanagh, A. S.; Wang, V.; Kummel, A. C.; George, S. M. Electron-Enhanced Atomic Layer Deposition of Ru Thin Films Using $Ru(DMBD)(CO)_3$ and Effect of Forming Gas Anneal. *J. Vac. Sci. Technol. A* **2023**, *41*, 062408.

(40) Puurunen, R. L. Surface Chemistry of Atomic Layer Deposition: A Case Study for the Trimethylaluminum/Water Process. *J. Appl. Phys.* **2005**, *97*, 121301.

(41) George, S. M. Atomic Layer Deposition: An Overview. *Chem. Rev.* **2010**, *110*, 111−131.

(42) Zywotko, D. R.; Zandi, O.; Faguet, J.; Abel, P. R.; George, S. M. ZrO_2 Monolayer as a Removable Etch Stop Layer for Thermal Al_2O_3 Atomic Layer Etching Using Hydrogen Fluoride and Trimethylaluminum. *Chem. Mater.* **2020**, *32*, 10055−10065.

(43) Mahuli, N.; Cavanagh, A. S.; George, S. M. Atomic Layer Deposition of Hafnium and Zirconium Oxyfluoride Thin Films. *J. Vac. Sci. Technol. A* **2021**, *39*, 022403.

(44) Knotter, D. M.; Denteneer, T. J. J. Etching Mechanism of Silicon Nitride in HF-Based Solutions. *J. Electrochem. Soc.* **2001**, *148*, F43−F46.

(45) Hilfiker, J. N.; Singh, N.; Tiwald, T.; Convey, D.; Smith, S. M.; Baker, J. H.; Tompkins, H. G. Survey of Methods to Characterize Thin Absorbing Films with Spectroscopic Ellipsometry. *Thin Solid Films* **2008**, *516*, 7979−7989.

(46) Junige, M.; Oddoy, T.; Yakimova, R.; Darakchieva, V.; Wenger, C.; Lupina, G.; Kitzmann, J.; Albert, M.; Bartha, J. W. Atomic Layer Deposition of Al_2O_3 on NF_3-Pre-Treated Graphene. *Proc. SPIE* **2015**, *9519*, 951915.

(47) Junige, M.; Löffler, M.; Geidel, M.; Albert, M.; Bartha, J. W.; Zschech, E.; Rellinghaus, B.; van Dorp, W. F. Area-Selective Atomic Layer Deposition of Ru on Electron-Beam-Written Pt(C) Patterns Versus SiO_2 Substratum. *Nanotechnology* **2017**, *28*, 395301.

(48) Richter, R. P.; Rodenhausen, K. B.; Eisele, N. B.; Schubert, M. Coupling Spectroscopic Ellipsometry and Quartz Crystal Microbalance to Study Organic Films at the Solid-Liquid Interface. In *Ellipsometry of Functional Organic Surfaces and Films*; Hinrichs, K., Eichhorn, K.-J., Eds.; Springer: Cham, Switzerland, 2018; pp 391−417.

(49) Colles, M. J.; Griffiths, J. E. Relative and Absolute Raman Scattering Cross Sections in Liquids. *J. Chem. Phys.* **1972**, *56*, 3384−3391.

(50) Burns, K. H.; Srivastava, P.; Elles, C. G. Absolute Cross Sections of Liquids from Broadband Stimulated Raman Scattering with Femtosecond and Picosecond Pulses. *Anal. Chem.* **2020**, *92*, 10686−10692.

(51) Habuka, H.; Otsuka, T. Reaction of Hydrogen Fluoride Gas at High Temperatures with Silicon Oxide Film and Silicon Surface. *Jpn. J. Appl. Phys.* **1998**, *37*, 6123−6127.

(52) Watanabe, D.; Aoki, H.; Itano, M.; Kezuka, T.; Kimura, C.; Sugino, T. High Selectivity (SiN/SiO_2) Etching Using an Organic Solution Containing Anhydrous HF. *Microelectron. Eng.* **2009**, *86*, 2161−2164.

(53) Helms, C. R.; Deal, B. E. Mechanisms of the HF/H_2O Vapor Phase Etching of SiO_2. *J. Vac. Sci. Technol. A* **1992**, *10*, 806−811.

(54) Holmes, P. J.; Snell, J. E. A Vapour Etching Technique for the Photolithography of Silicon Dioxide. *Microelectron. Reliab.* **1966**, *5*, 337−341.

(55) Kang, J. K.; Musgrave, C. B. The Mechanism of HF/H_2O Chemical Etching of SiO_2. *J. Chem. Phys.* **2002**, *116*, 275−280.

(56) McIntosh, R.; Kuan, T.-S.; Defresart, E. Hydrogen Fluoride Vapor Etching for Pre-Epi Silicon Surface Preparation. *J. Electron. Mater.* **1992**, *21*, 57−60.

(57) Watanabe, H.; Kitajima, H.; Honma, I.; Ono, H.; Wilhelm, R. J.; Sophie, A. J. L. Influence of Water Adsorption/Desorption Processes on the Selectivity of Vapor HF Etching. *J. Electrochem. Soc.* **1995**, *142*, 1332−1340.

(58) Reif, J.; Knaut, M.; Killge, S.; Albert, M.; Mikolajick, T.; Bartha, J. W. *In Situ* Studies on Atomic Layer Etching of Aluminum Oxide Using Sequential Reactions with Trimethylaluminum and Hydrogen Fluoride. *J. Vac. Sci. Technol. A* **2022**, *40*, 032602.

(59) Murdzek, J. A.; Rajashekhar, A.; Makala, R. S.; George, S. M. Thermal Atomic Layer Etching of Amorphous and Crystalline Al_2O_3 Films. *J. Vac. Sci. Technol. A* **2021**, *39*, 042602.

(60) Knotter, D. M. Etching Mechanism of Vitreous Silicon Dioxide in HF-Based Solutions. *J. Am. Chem. Soc.* **2000**, *122*, 4345−4351.

(61) Knotter, D. M. The Chemistry of Wet Etching. In *Handbook of Cleaning for Semiconductor Manufacturing*; Reinhardt, K. A., Reidy, R. F., Eds.; Scrivener Publishing: Salem, MA, USA, 2011; pp 95−141.

(62) Torek, K.; Ruzyllo, J.; Grant, R.; Novak, R. Reduced Pressure Etching of Thermal Oxides in Anhydrous HF/Alcoholic Gas Mixtures. *J. Electrochem. Soc.* **1995**, *142*, 1322−1326.

(63) Lee, Y.-I.; Park, K.-H.; Lee, J.; Lee, C.-S.; Yoo, H. J.; Kim, C.-J.; Yoon, Y.-S. Dry Release for Surface Micromachining with HF Vapor-Phase Etching. *J. Microelectromech. Syst.* **1997**, *6*, 226−233.

(64) Guillemin, S.; Mumbauer, P.; Radtke, H.; Fimberger, M.; Fink, S.; Kraxner, J.; Faes, A.; Siegert, J. Etching Mechanisms of SiO_2 and SiN_x:H Thin Films in HF/Ethanol Vapor Phase: Toward High Selectivity Batch Release Processes. *J. Microelectromech. Syst.* **2019**, *28*, 717−723.

(65) Jang, W. I.; Choi, C. A.; Lee, M. L.; Jun, C. H.; Kim, Y. T. Fabrication of MEMS Devices by Using Anhydrous HF Gas-Phase Etching with Alcoholic Vapor. *J. Micromech. Microeng.* **2002**, *12*, 297−306.

(66) Hattori, T.; Kobayashi, H.; Ohtake, H.; Akinaga, K.; Kurosaki, Y.; Takei, A.; Sekiguchi, A.; Maeda, K.; Takubo, C.; Yamada, M. Highly Selective Isotropic Gas-Phase Etching of SiO_2 Using HF and Methanol at Temperatures −30°C and Lower. *Jpn. J. Appl. Phys.* **2023**, *62*, SI1001.

(67) Klaus, J. W.; Sneh, O.; George, S. M. Growth of SiO_2 at Room Temperature with the Use of Catalyzed Sequential Half-Reactions. *Science* **1997**, *278*, 1934−1936.

(68) Klaus, J. W.; George, S. M. Atomic Layer Deposition of SiO_2 at Room Temperature Using NH_3-Catalyzed Sequential Surface Reactions. *Surf. Sci.* **2000**, *447*, 81−90.

(69) Du, Y.; Du, X.; George, S. M. Mechanism of Pyridine-Catalyzed SiO_2 Atomic Layer Deposition Studied by Fourier Transform Infrared Spectroscopy. *J. Phys. Chem. C* **2007**, *111*, 219−226.

(70) Parks, G. A. The Isoelectric Points of Solid Oxides, Solid Hydroxides, and Aqueous Hydroxo Complex Systems. *Chem. Rev.* **1965**, *65*, 177−198.